Bilayers as Phase Transfer Agents for Nanocrystals Prepared in Nonpolar Solvents

Arjun Prakash,[†] Huiguang Zhu,[‡] Christopher J. Jones,[‡] Denise N. Benoit,[‡] Adam Z. Ellsworth,[‡] Erika L. Bryant,[‡] and Vicki L. Colvin[†,‡,*]

[†]Department of Chemical and Biomolecular Engineering and [‡]Department of Chemistry, Rice University, Houston, Texas 77005

ABSTRACT The effective water dispersion of highly uniform nanoparticles synthesized in organic solvents is a major issue for their broad applications. In an effort to overcome this problem, iron oxide and cadmium selenide nanocrystals were surrounded by lipid bilayers to create stable, aqueous dispersions. The core inorganic particles were originally generated in oleic acid and 1-octadecene. When these organic solutions were mixed with water and a sparing amount of excess fatty acid, up to 70% of the nanoparticles transferred into the aqueous phase. This simple approach was applied to two different nanocrystal types, and nanocrystal diameters ranging from 5 to 15 nm. In all cases, the resulting materials were stable, nonaggregated suspensions that retained their original magnetic and optical properties. The phase transfer efficiency is maximum when very little oleic acid is added (*e.g.* 0.2 w/w %). At higher concentrations, above the critical micelle concentration, the formation of micelles begins to compete with bilayer generation leading to less effective phase transfer. Unlike other approaches for water dispersion that rely on amphiphiles with significant water solubility, the fatty acids used in this work are only sparingly soluble in water. As a result, there is minimal dynamic exchange between free and bound surface agents and the resulting aqueous solutions contain little residual free organic carbon. Thermogravimetric analysis (TGA) confirmed the presence of bilayers around the nanocrystal cores. The particle size, size distribution, process yield, and colloidal stability were found using a suite of methods including transmission electron microscopy, small angle X-ray scattering, dynamic light scattering, inductively coupled plasma—optical emission spectroscopy, and ultraviolet—visible spectroscopy. Bilayer—nanocrystal complexes possess many of the same size-dependent features as the original materials, and as such offer new avenues for exploring and exploiting the interface between nanocrystals and biology.

KEYWORDS: bilayer-nanocrystal · iron oxide · quantum dots · SAXS · fatty acid · nonpolar

The phase transfer of nanoparticles from nonpolar to polar suspensions remains an outstanding challenge for material chemists. The best quality nanocrystals, with respect to uniformity, size control, and crystallinity, are generally formed in organic solutions at elevated temperatures.[1−5] These synthetic methods produce nanomaterials as diverse as gold, cadmium selenide, and iron oxide which as a consequence of their formation conditions possess surfaces that terminate in organic, nonpolar moieties. However, to apply the unique optical and magnetic properties of these nanocrystals often requires surface modifications that yield well dispersed and nonaggregated materials stable in water.[6−9] Nanoscale iron oxides, for example, in water purification as well as magnetic resonance imaging must be used in aqueous solutions.[8,10,11] Quantum dots find enormous application as biological imaging agents, a technology that requires compact and isolated particles whose surfaces are compatible with a variety of biological fluids.[12−14] These and other uses for nanocrystals have sustained interest in this topic for nearly a decade; researchers have focused on methods that are both efficient in their transfer of nanocrystals and capable of preventing material aggregation and dissolution.[5,15−20]

Many of the existing strategies for nanocrystal phase transfer use lipids as essential components of amphiphilic surface coatings.[5,7,21] One commercial quantum dot material reports the use of a proprietary PEG−lipid to create a stable and water-soluble material.[22] In these examples, the lipids—typically fatty acids—function as the nonpolar constituent of larger amphiphiles (*e.g.*, surfactants). Their hydrophobic tail interacts with the nanocrystal's nonpolar organic surface and leads to a full encapsulation of the core and its original coating. The hydrophilic end of the amphiphile is thus left to stabilize the new surface and renders the material polar and fully dispersed in water. This encapsulation approach ensures that the nanoparticle surfaces are never stripped of their original organic coatings. As a result, particle aggregation is minimized due to the presence of steric stabilization during the entire phase transfer process. Also, in the case of quantum dots, encapsulation is strongly preferred as it prevents degradation of the desirable optical properties.[5,23] Nanocrystal encapsulation can be problematic in some

*Address correspondence to colvin@rice.edu.

Received for review April 14, 2009 and accepted July 07, 2009.

Published online July 13, 2009.
10.1021/nn900373b CCC: $40.75

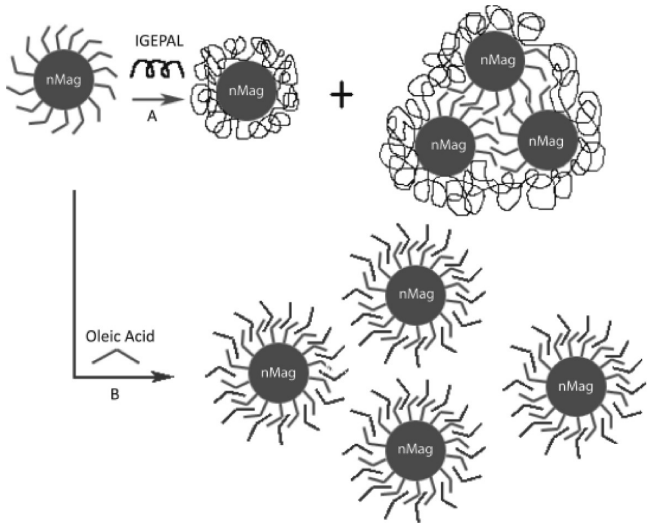

Figure 1. Illustration of the aqueous transfer of iron oxide nanoparticles (nMag) *via* both (A) addition of IGEPAL CO 630 surfactant; polymeric surfactants can result in the formation of clusters of nanoparticles in the final aqueous suspensions (B) bilayer formation.

circumstances as the size of the resulting core and surface treatment can be much larger than the starting organic material; moreover, it often requires expensive or customized copolymers and surfactants.[9,20] Still there are good examples of phase transfer strategies that can produce nonaggregated and stable nanocrystal dispersions in water.[15−18,20,24] These efforts include encapsulation using polymers (*e.g.,* polyacrylic acid, polyethylene glycol) and ligand exchange using moieties such as bifunctional thiols.[25,26]

Whatever the surface agent selected to affect a phase transfer, it is generally desirable that the resulting nanocrystal suspensions contain little free surfactant or other organic species. Such a criterion is particularly important for biomedical and toxicological studies.[27−29] Conventional practice relies on sedimentation or filtration to concentrate and purify nanoparticles. These treatments can be intrinsically limited if nanocrystal surface coatings are themselves soluble in water. Unless cross-linked or otherwise irreversibly attached to the nanoparticle, most surface-bound amphiphiles will exist in equilibrium with their free form.[30] As a result, coatings can be removed if nanocrystals are repeatedly washed or diluted. Moreover, the dynamic exchange of the encapsulating agents can result in an adventitious adsorption of other materials, yielding a nanocrystal interface quite different from the one originally engineered.[31] Perhaps the most significant consequence of labile surface coatings is that nanocrystal suspensions must necessarily contain some quantity of the soluble, free surfactant.

These issues motivated our interest in an alternative approach to nanoparticle phase transfer. Our goal was to form small, stable, and nonaggregated nanocrystals in water whose size-dependent properties were preserved; however, we wanted to achieve these features by using a surface coating that in its pure form would have extremely low water solubility. To achieve this end, we use a phase transfer process that generates a fatty acid bilayer at the nanoparticle interface (Figure 1B). The term "bilayer" in this work is directed toward lipid bilayers, where both the layers are made up of the same moiety. We selected a fatty acid, oleic acid, whose monomer is highly insoluble in water. However, in its bilayer form it presents a stable and polar interface well suited for a variety of physiological environments. Our methods were inspired by efforts to sterically stabilize iron oxide colloids. For colloids formed in water, phase transfer due to bilayer formation is not the goal as it is in this work. Instead, bilayers are used to slow or reverse colloidal particle aggregation; many water-soluble amphiphiles have been demonstrated for this purpose including SDBS,[32] dodecanoic acid,[33] alkanoic acids,[7,21] phospholipids,[34] and PLURONIC block copolymers.[35] This literature provides an important conceptual foundation for this effort and offers highly relevant examples of bilayer-nanoparticle characterization.

Here we show the results of a versatile and simple approach to the generation of bilayer stabilized nanocrystals, entities that we term "bilayer−nanocrystal complexes". While most of the examples provided in this effort center on iron oxide nanocrystals, we also have explored the stabilization of quantum dots as illustrated in our study of phase transfer efficiency. The resulting materials possess small hydrodynamic sizes and are stable under a wide range of physiological conditions. SAXS indicates that in contrast to systems stabilized by polymeric surfactants, bilayer−nanocrystal complexes are nonaggregated in water. Little free fatty acid or other organic carbon is measurable in the nanocrystal aqueous suspensions, a result anticipated given the low aqueous solubility of free oleic acid. Bilayer nanocrystal complexes retain their size dependent physical properties in water.

RESULTS AND DISCUSSION

This work focuses on a relatively unexplored avenue for creating stable aqueous suspensions of nanocrystals from organic solutions: namely, the generation of fatty acid bilayers around the original hydrophobic particles. Figure 1B illustrates the process studied in this work and contrasts it to the more conventional use of polymeric surfactants (Figure 1A) to affect nanocrystal phase transfer. Both methods use amphiphiles to change the interfacial chemistry of particles from nonpolar to polar. The standard approach relies on the hydrophobic blocks of amphiphilic polymers to wrap the nonpolar surfaces of particles or groups of particles. Of interest here is the application of molecular fatty acids, identical to those already present at quantum dot and iron oxide interfaces, as phase transfer agents. In the nonpolar nanocrystal solutions these fatty acids form dense and compact coatings with the hydrocarbon tail

oriented toward the solution phase. We reasoned that if slightly more fatty acid is added, and the systems appropriately mixed, a second layer of fatty acid could be laid down on top of the original one. The process would result in the formation of a bilayer−nanocrystal complex that would present polar groups at the particle interface and subsequently lead to particle dispersion in water.

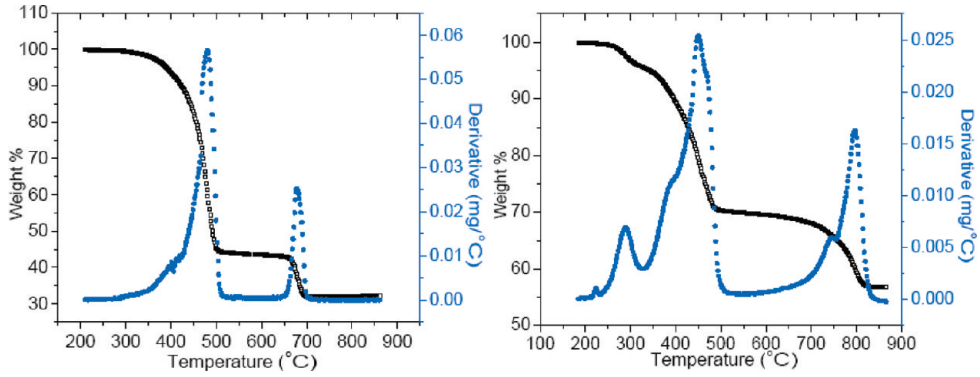

Figure 2. Thermo-gravimetric analysis (TGA) curves for 10 nm (left) and 17 nm (right) iron oxide nanocrystals. The black dots indicate the percent weight as a function of temperature and the weight loss derivative is indicated in blue. In both the cases, sample mass remained constant while cooling from 900 to 50 °C.

To explore this approach, oleic acid—a C18 unsaturated fatty acid—was added as a phase transfer agent to an oil/water mixture of iron oxide or cadmium selenide nanocrystals. The choice of oleic acid was motivated by several factors: its hydrophobic tail is long enough to interact with existing hydrophobic coatings; it has poor micelle forming ability due to the presence of a double bond; and finally it is a simple choice as oleic acid is the native fatty acid used in the nanocrystal synthesis.[21] Under the appropriate mixing conditions, for example probe sonication, the colored nanocrystals could be transferred from the organic to aqueous layers with high (>70%) efficiency. Several characterization methods were then applied to confirm that the surfaces of the nanoparticles in water were covered in bilayers; among these thermo-gravimetric analysis (TGA) is the most conclusive for these structures.

During controlled heating of sample residues, two distinct weight loss peaks can be observed. These correlate well in temperature to those reported for fatty acid double layers in a variety of environments (Figure 2).[7] The mass loss between 400 and 500 °C corresponds to the desorption of the outer layer of oleic acid; as expected, it occurs at a temperature slightly higher than the boiling point of neat oleic acid or 360 °C at 760 mm Hg.[36] A second inflection point occurs between 650 and 800 °C. This feature arises from the loss of more tightly bound oleic acid. This inner layer of oleic acid is thought to be stabilized *via* a complex between iron(II) and the carboxylate groups of oleic acid.[7,9] As a result, it can only be removed from the surface at higher temperatures. Also, we note that the weight loss difference between the outer and inner layers can be semiquantitatively attributed to the higher curvature of the smaller 10 nm particle in comparison with the bigger 17 nm particle. The coincidence of the TGA peak temperatures in these samples with that reported previously for bilayers, both on surfaces and colloids, is strong evidence that under our process conditions the materials are stabilized by oleic acid bilayers.[37]

The formation of bilayers around the nanocrystal surfaces is also consistent with the strong sensitivity of process yield to fatty acid concentration (Figure 3). A striking feature of these data is the extremely low quantities of fatty acid required to obtain high phase transfer yields (Figure 3). For both quantum dots and iron oxide nanocrystals, over 70% of the material is transferred from hexanes to water after the addition of only 0.2 w/w% oleic acid. This is in stark contrast to particle stabilization with IGEPAL CO 630 which requires more than 10 w/w% for reasonable phase transfer yields.[10] This observation is likely due to the competition between oleic acid micelle and bilayer formation. At or near its critical micelle concentration (CMC), oleic acid can form micelles in water, and this process would remove bilayer material from the surface and reduce the solubility in water.[38,39] As a result, the optimal phase transfer efficiency is obtained near the CMC for oleic acid. This observation may explain why reports of bilayer phase transfer methods for highly uniform nanocrystals are limited: conventional practice involves the addition of a vast excess of phase transfer agent to a suspension in

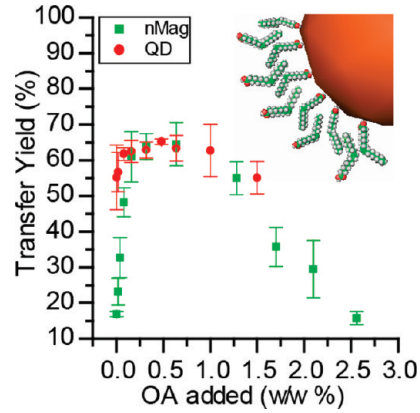

Figure 3. Variation of the transfer yield of iron oxide (nMAG) nanoparticles and quantum dots (QD) from hexanes into water as a function of oleic acid (OA) concentration. Inset: Scale depiction of a 10 nm diameter nanocrystal coated with a bilayer. Iron oxide concentration was obtained by ICP analysis and quantum dot concentration was obtained *via* absorbance.

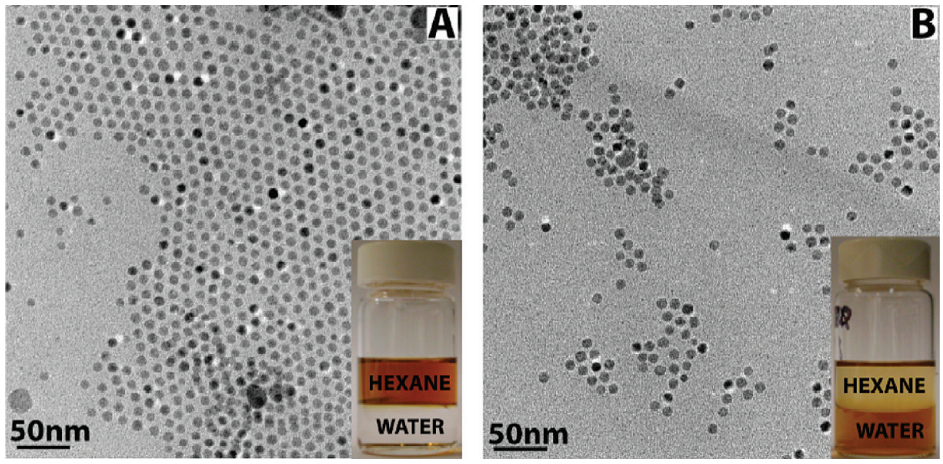

Figure 4. Transmission electron micrographs of iron oxide nanoparticles (A) in organics (9.6 ± 1.0 nm), (B) phase transferred into water *via* bilayer formation (10 ± 1 nm). Inset pictures show phase separated mixtures with water phase at the bottom and hexane phase at the top. As is clear the phase transfer efficiency is on the order of 70% as some color remains in the organic phase. More than 1000 particles were measured to capture both the average size and the size distribution.

order to ensure an efficient process. As apparent in Figure 3, such an approach would depress the transfer efficiencies substantially. In general, if bilayer formation is desired it is best to work with fatty acid concentrations (0.7−3.5 mM for oleic acid) that are at or below the critical micelle concentration.[39] At their highest transfer yields, the molar ratio of oleic acid to nanoparticles was found to be 90 for 10 nm iron oxide and 17 for 4 nm quantum dots. This observation between the two nanoparticle systems could be attributed to the order of magnitude difference in their surface areas.

Also notable in Figure 3 is the similarity between the process yield for both quantum dots and iron oxide nanocrystals. Not only is the core composition different in these two cases, but the core diameters are also very different (*e.g.*, 4 nm diameter as opposed to 10 nm diameter). Still the behavior and optimization is comparable suggesting that as long as particles possess a hydrophobic surface, the addition of small amounts of fatty acid may be suitable for creating water stable dispersions.

The total organic carbon (TOC) found free in solution for the oleic acid stabilized nanoparticles is just 9 ppm, 3 orders of magnitude less than that found for equivalent polymer encapsulated (IGEPAL CO 630) materials. This observation can be explained by the different solubilities of oleic acid *versus* conventional phase transfer agents. Large amounts of polymeric surfactants like IGEPAL are required to affect nanoparticle phase separation because these materials alone have high solubility in water. An excess of free polymer in the aqueous suspensions ensures a complete and stable surface coating. In contrast, oleic acid is virtually insoluble in water (HLB value of 1) and once incorporated into a bilayer structure will not appreciably desorb from the surface.[33] The price paid for an insoluble surface stabilizing agent is the challenge associated with combining the original hydrophobic nanoparticles, free oleic acids, and water. Here we overcome this kinetic barrier by using a brief ultrasonication process which quickly mixes the various components and results in stable aqueous suspensions. While our phase transfer yields are quite high, on the order of 70%, they are not 100% effective, and this is likely due to the challenges of mixing the disparate starting materials (Figure 3). We note that it may also be possible to replace ultrasonication with elevated temperatures for more polar fatty acids and their salts.[7]

An important concern for applications of nanocrystals in water is that the phase transfer process should preserve the original quality of the material as well as prevent particle aggregation. The first issue is of particular concern in this process as it relies on probe sonication to ensure adequate mixing of the insoluble fatty acids, nanocrystals, and water. The preparation of nanocrystals in organic media affords a great deal of control over nanocrystal nucleation and growth, and as a result the as-synthesized nanocrystals possess symmetric shapes, narrow size distributions, and high crystallinity (Figure 4A). These desirable features remain unchanged after the phase transfer process (Figure 4B). Most notably, each particle is well separated from its neighbors in the microscopy images, suggesting that an organic coating is associated with individual particles. Particle aggregation is not prevalent in the dried films. This observation is supported by the high clarity of the suspensions and their apparent lack of sedimentation over months (insets Figure 4).

Direct evidence that bilayer−nanocrystal complexes are not aggregated is found in an analysis of their small-angle X-ray scattering (SAXS) profiles. This method is sensitive to the presence of aggregates from 2−10 particles across, and complements well the visual observations and microscopic analysis in Figure 4.[40] Figure 5A,B presents the SAXS profiles for bilayer-coated iron oxide nanocrystals of 10 and 17 nm core diameters in water. The inverted scattering minima at low angles are very sensitive to the particle size distribution, and their appearance in the raw data confirm the finding from TEM that these are highly uniform samples. Models for X-ray scattering of small particles can be fit to these data to obtain more quantitative information, and these take as inputs the density, expected size, and size distribution of the particles.[41] The best fits to the scattering data are shown as solid lines and the resulting overall size distributions are shown in the figure inset. As ex-

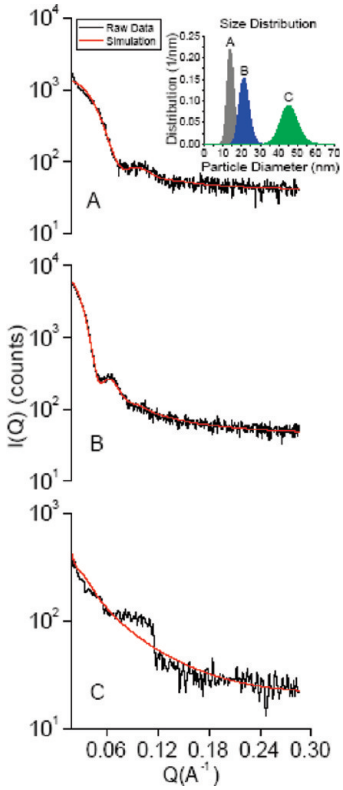

Figure 5. Small angle X-ray scattering profiles (in black) with simulated fits (in red) for iron oxide nanoparticles in water: (A) 10 nm core (bilayer coated), (B) 17 nm core (bilayer coated), (C) 10 nm core (polymer coated). Inset: corresponding size distributions.

pected, the larger core sizes lead to greater diameters; moreover, the average sizes are representative of nonaggregated and fully isolated nanoparticles. These basic conclusions were confirmed by dynamic light scattering data (Table 1) which provides a semiquantitative measurement of the average hydrodynamic diameter of nanocrystals directly in suspension.

The hydrodynamic diameters of these materials are in good agreement with what is expected for an inorganic core surrounded by a fatty acid bilayer (Table 1). In this analysis, dimensions found from multiple characterization methods were compared to extract the effective thickness of the bilayers. TEM provides the inorganic core diameter; SAXS analysis provides a measure of the extent of the core and the dense organic coatings; and finally, DLS data reports the full hydrodynamic diameter of the bilayer−nanocrystal complex and associated hydration shell. The diameters obtained *via* SAXS and DLS for bilayer−nanocrystal complexes (sample A and sample B) are larger than the inorganic core as expected; the 4.6 nanometer difference (average of samples A and B shell size) between the inorganic cores and the bilayer−nanoparticle complex can be attributed to the oleic acid bilayer. This corresponds to a surface coating thickness of about 2.3 nm which is comparable to the thickness of C-18 chain bilayers measured in other similar systems.[42] Both in these systems, as well in other oleic acid bilayers, there is a large degree of interpenetration of the C-18 chains—a feature depicted schematically in Figure 3.[7] Sample B corresponds to 17 nm core iron oxide particles coated with oleic acid bilayer. Similar bilayer dimensions were obtained *via* SAXS and DLS for this case, and these are consistent with that of the smaller sample A.

TABLE 1. Diameters of Iron Oxide Nanoparticles Dispersed in Water[a]

sample	A (nm)	B (nm)	C (nm)
TEM (core)	10.0 ± 1.2	16.6 ± 2.3	10.0 ± 1.2
SAXS (core + shell)	14.3 ± 1.8	21.5 ± 2.6	49.0 ± 4.8
DLS (hydrodynamic)	14.2 ± 2.6	26.3 ± 4.1	154.1 ± 15.6

[a]Obtained by TEM (particle core), SAXS (particle core + shell) and DLS (hydrodynamic) for particles of size (A) 10 nm, bilayer coated; (B) 17 nm, bilayer coated; and (C) 10 nm, polymer coated.

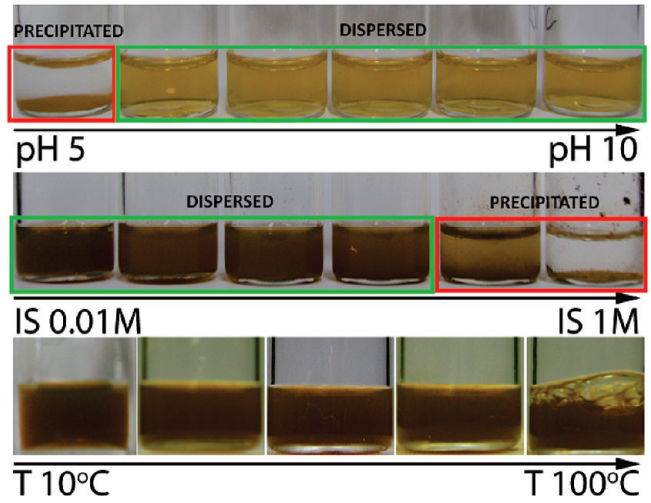

Figure 6. Iron oxide nanocrystal suspensions (10 nm core size) under varying solution phase conditions. Particles that were visibly sedimented or cloudy are surrounded by a red box; solutions with unchanged visual appearance are surrounded in green. These charge-stabilized materials become unstable at low pH, when the fatty acid coatings are protonated (top panel) as well as at high ionic strengths in NaCl (middle panel). Temperature has remarkably little effect on the systems.

An important feature of bilayer−nanocrystal complexes highlighted by Table 1 is that they form compact structures in aqueous suspensions. Typically, the bilayer−nanocrystal complexes are are only 4.6 nm larger than the core nanocrystal. Quantum dots stabilized by amphiphilic surfactants, for example, can possess hydrodynamic diameters nearly 5−10 times larger than their core diameter.[24,43,44]

Bilayers produced *via* oleic acid have remarkable chemical and thermal stability. The formation of a bilayer on the nanocrystal surface leads to a pH-dependent charge stabilization confirmed by zeta potential measurements (−55 mV at a pH of 6.0). Figure 6 shows the visual appearance of bilayer−nanocrystal complex suspensions under different conditions of pH, ionic strength, and temperature. As expected for these systems, in acidic conditions the surface groups are pro-

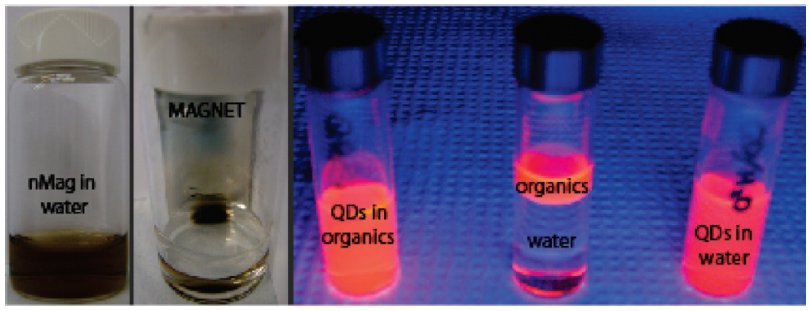

Figure 7. Optical and magnetic properties of bilayer−nanocrystal complexes are similar to the original materials. On the far left panels, a strong permanent magnet is able to concentrate the iron oxide materials (nMAG) much as is observed in hexanes. On the right panel, the fluorescence of quantum dots (QD) is relatively unchanged after the formation of a bilayer and the transfer of the material into water.

tonated; above the pK_a of oleic acid (≈5.0); however, the nanocrystals are quite stable.[45] The addition of salts to these suspensions can result in the precipitation of nanocrystal aggregates; the middle panel of Figure 6 illustrates that above 250 mM the electrostatic repulsion is effectively shielded and interparticle aggregation becomes substantial. DLS confirms these visual observations. While the materials are somewhat sensitive to both charge and pH, they are remarkably stable over a variety of temperatures (bottom, Figure 6).

A delineation of the unique and valuable optical and magnetic properties of nanocrystals has been the subject of extensive prior work.[5,10,14,46] Here, we simply confirm that the important physical properties of both of these model systems remain unchanged after transfer into water (Figure 7). Nanocrystalline iron oxide phase transferred into water can be captured by an external magnetic field; the time for capture and the overall efficiency of the process is unchanged as would be expected given the physical characterization of the materials (Figure 4). Figure 7 also illustrates that the optical properties of quantum dots before and after bilayer stabilization are relatively unchanged. Most importantly, the quantum yield for these quantum dots systems remains within 20% of its original value after phase transfer. Complete analysis of the optical and magnetic properties of these complexes is the subject of future work. This data is presented here only to establish that the process does not significantly alter the core nanocrystal features.

Finally, to identify the advantages of a bilayer stabilization approach we compare these results to those found using a conventional polymeric surfactant, IGEPAL CO 630. Figure 5C shows that these surfactants when applied to iron oxide nanocrystals result in particle aggregation; larger amphiphilic phase transfer agents have been reported to encapsulate multiple particles.[20,37] This results in polydisperse groupings of iron oxide nanocrystals. Also, corresponding DLS diameters (Table 1, sample C) show a significant increase over the particle core size, indicating the presence of aggregates in polymer stabilized materials. These observations highlight the significant challenges faced in preventing aggregation of these magnetic materials during phase transfer. The approach outlined in this paper, in contrast, is successful in generating isolated magnetic nanocrystals as well as quantum dots.

CONCLUSIONS

Lipid bilayers prepared from a water insoluble fatty acid can be generated around both iron oxide and cadmium selenide nanocrystals. These surface coatings form around nanoparticles after mixing hexane solutions of the materials, free fatty acids and water; thermogravimetric analysis confirms the existence of lipid bilayers. The bilayer thickness on a variety of nanocrystal cores was deduced from both dynamic light scattering and small-angle X-ray scattering; typical values of 2.2−2.5 nanometer are consistent with those reported for comparable immobilized bilayers. An interesting finding is that bilayer formation is only successful when a small amount (0.2 w/w %) of oleic acid is incorporated into the organic solutions. Phase transfer efficiencies may be depressed at higher concentrations due to the self-association of the fatty acids into micelles. An important advantage of using a highly insoluble fatty acid to affect nanocrystal phase transfer is the resulting purity of the aqueous suspension: once captured into a lipid bilayer around a nanoparticle, there is no driving force for the desorption of free fatty acid. Small angle X-ray scattering of the aqueous suspensions reveals that the materials are uniform and nonaggregated. The resulting bilayer−nanoparticle complexes are highly stable over a wide range of temperatures, ionic strength, and pH as expected for a moderately charged interface. Bilayer formation does not change the essential size-dependent properties of nanocrystals and offers several advantages over conventional encapsulation strategies.

METHODS

Nanocrystal Synthesis. Iron oxy-hydrate (FeO(OH) iron(III) oxide, hydrated; catalyst grade, 30−50 mesh;), 1-octadecene (ODE 90%), cadmium oxide (CdO 99.99%), selenium powder (Se 100 mesh 99%), trioctylphosphine (TOP 99%), oleic acid (90%), and nitric acid (trace metal grade) were all purchased from SIGMA-Aldrich. The 1 μm PTFE AERODISC syringe filter was purchased from PALL LIFE SCIENCE and a 0.2 μm NYL syringe filter was purchased from WHATMAN.

Iron oxide nanoparticles were synthesized by the thermal decomposition of iron carboxylate salts.[2,47] A mixture of 0.178 g of FeO(OH), 2.26 g oleic acid, and 5.0 g of 1-octadecene was stirred and purged with nitrogen; moderate heating up to 280 °C in a three neck-flask led to the formation of an orange solution

thought to contain iron carboxylates. Further heating to 320 °C led to a decomposition of this precursor and the generation of brown-black iron oxide nanocrystals. The reaction product was soluble in hexane because of the adsorption of oleic acid to the nanocrystal surface *via* polar, carboxylate groups.

The iron oxide nanocrystals were purified by repeated cycles of precipitation and sedimentation followed by dispersion in hexane. Reaction products were treated with a 1:1 volumetric amount of acetone and methanol leading to the formation of visible aggregates; these were collected *via* centrifugation in a pellet and could be dispersed back into hexanes. This procedure was repeated five times to remove unreacted iron salts, 1-ODE, or unbound oleic acid. Purified nanocrystal solutions in hexanes could be digested by strong nitric acid and analyzed for their iron content with atomic emission spectroscopy (ICP-OES). Using the average diameter of the material obtained from TEM, and the density of iron oxide (5.17 g/cm^3), the atomic concentration of iron could be converted into a nanoparticle concentration.

CdSe nanocrystals were prepared by heating a stirred mixture of 0.3 g of CdO and 2.7 g of oleic acid in a 100 mL three-neck flask at 200 °C until a transparent liquid was obtained.[48] After cooling to room temperature, 15 g of oleic acid and 30 g of ODE were added and the mixture heated to 100 °C under vacuum for 40 min. The solution was then purged with ultrapure N_2 and heated to 300 °C. An injection solution, prepared by mixing 10.68 g of Se/TOP (10 wt %) and 4.13 g of ODE, was swiftly injected into the flask with a 20 mL syringe fitted with a large bore needle. After cooling to room temperature, the crude quantum dots were precipitated by the addition of acetone and methanol, in a fashion similar to that used for the iron oxide. These pellets could be isolated and purified after repeated centrifugation at 3500*g* followed by redispersion into hexanes. The final purified nanocrystal pellet was ultimately redispersed in hexane, filtered through 1 μm PTFE syringe filter, and stored in the dark. Quantum dot concentrations were estimated from absorbance data using methods published elsewhere.[49]

Phase Transfer of Nanocrystals. Oleic acid was added in variable amounts (0.5−300 μL) to 1.0 mL of purified nanocrystal suspensions in hexanes (typically 1 g nanoparticle/L). The resulting solution was then sonicated in a bath for 1 min with no visible change in appearance (FS6 sonicator from FISCHER SCIENTIFIC). Next, 10 mL of ultrapure water (MILLIPORE, 18.2MΩcm) was then added to the hexane solution resulting in an obvious phase separation between the clear water and colored nonpolar solution. To affect the transfer of material from hexanes into water, this solution was subjected to sonication *via* a probe (UP 50H probe sonciator from DR.HIELSCHER) for 5 min at 50% amplitude and full cycle. Care was taken to ensure that the tip of the probe, where the power is the highest, was located near the interfacial region between the hexanes and water phase. Immediately after sonication a cloudy and colored solution was obtained, but if left to sit undisturbed for 1 day the mixture phase separated with the colored nanoparticles appearing in the bottom, aqueous fraction. This layer was collected and the nanoparticles purified *via* centrifugation at 3500*g* for 15 min, followed by redispersion and filtration through a syringe filter (pore size of 0.2 μm, Whatman-NYL). The filtered product was a clear, colored suspension that could be further concentrated (typically 10×) *via* rotary evaporation. The above procedure was also used to phase transfer cadmium selenide nanocrystals. Methods to describe the phase transfer using IGEPAL CO 630 are described elsewhere.[10]

Characterization of Nanocrystals. Small angle X-ray scattering (SAXS) profiles were obtained on a RIGAKU SMARTLAB system operating in transmission mode with a line collimation setup. A capillary tube (0.8 mm diameter) was filled with a sample, and the low angle scattering was collected from 2θ values of 0.15−4 degrees with a Cu Kα X-ray beam of wavelength 1.54 Å. The X-rays were generated at 40 kv and 44 mA. Typical data collection times were on the order of 2 h. The raw scattering data was analyzed using Rigaku's NANOSOLVER software using a split interval of 30 with low slit correction factor.

Dynamic light scattering (DLS) data was collected using a BROOKHAVEN instrument equipped with a BI-9000AT digital autocorrelator using a monitoring wavelength of 656 nm. Standard 1.5 mL poly methacrylate cuvettes were used as sample holders and each sample was analyzed for 4 min to obtain a minimum intensity of 200 000 cps. A histogram of the particle diameter distribution was obtained *via* a "Contin" fit to the raw autocorrelation data.

Transmission electron microscopy (TEM) was carried out using JEOL 2100 field emission gun TEM at 200 kV with a single tilt holder using 300 mesh copper grids with holey carbon from Ted Pella Inc. Thermogravitmetric analysis (TGA) was carried out using TA INSTRUMENTS SDT 2960 simultaneous DSC-TGA instrument with sample deposited in a platinum pan. Samples were maintained at 150 °C for 5 h for removal of any associated solvent/moisture before further heating. The samples were then heated to 900 °C at the rate of 50 °C/min. UV−visible spectroscopy was carried out using Cary 5000 VARIAN UV−vis−NIR spectrophotometer with 1.5 mL polymethacrylate cuvettes used as sample holders. All sizing data with respective significant figures were reported with error bars representing their standard deviation. Inductively coupled plasma (ICP) analysis was carried out using PERKIN ELMER ICP−OES instrument equipped with autosampler. Total organic carbon content of the supernatant was computed using SHIMADZU TOC analyzer after sedimentation of particle suspension (1 mL of 1 μM) (BECKMAN-COULTER OPTIMA L-80XP ultracentrifuge) at 118 000 g for 4 h at 25 °C.

Acknowledgment. This work was supported by the Center for Biological and Environmental Nanotechnology (NSF grant EEC-0647452) and Robert A. Welch Foundation (C-1342). We thank C. T. Yavuz, J. T. Mayo, M. S. Wong, J. Fortner, and R. Crouse for their advice and support.

REFERENCES AND NOTES

1. Kim, S.; Lim, Y. T.; Soltesz, E. G.; De Grand, A. M.; Lee, J.; Nakayama, A.; Parker, J. A.; Mihaljevic, T.; Laurence, R. G.; Dor, D. M.; *et al.* Near-Infrared Fluorescent Type II Quantum Dots for Sentinel Lymph Node Mapping. *Nat. Biotechnol.* **2004**, *22*, 93–97.
2. Yu, W. W.; Falkner, J. C.; Yavuz, C. T.; Colvin, V. L. Synthesis of Monodisperse Iron Oxide Nanocrystals by Thermal Decomposition of Iron Carboxylate Salts. *Chem. Commun.* **2004**, 2306–2307.
3. Battaglia, D.; Peng, X. G. Formation of High Quality InP and InAs Nanocrystals in a Noncoordinating Solvent. *Nano Lett.* **2002**, *2*, 1027–1030.
4. Murray, C. B.; Norris, D. J.; Bawendi, M. G. Synthesis and Characterization of Nearly Monodisperse CdE (E = S, Se, Te) Semiconductor Nanocrystallites. *J. Am. Chem. Soc.* **1993**, *115*, 8706–8715.
5. Dubertret, B.; Skourides, P.; Norris, D. J.; Noireaux, V.; Brivanlou, A. H.; Libchaber, A. *In Vivo* Imaging of Quantum Dots Encapsulated in Phospholipid Micelles. *Science* **2002**, *298*, 1759–1762.
6. Woo, K.; Hong, J. W. Surface Modification of Hydrophobic Iron Oxide Nanoparticles for Clinical Applications. *IEEE Trans. Magn.* **2005**, *41*, 4137–4139.
7. Shen, L. F.; Laibinis, P. E.; Hatton, T. A. Bilayer Surfactant Stabilized Magnetic Fluids: Synthesis and Interactions at Interfaces. *Langmuir* **1999**, *15*, 447–453.
8. Qin, J.; Laurent, S.; Jo, Y. S.; Roch, A.; Mikhaylova, M.; Bhujwalla, Z. M.; Muller, R. N.; Muhammed, M. A High-Performance Magnetic Resonance Imaging T-2 Contrast Agent. *Adv. Mater.* **2007**, *19*, 1874–1878.
9. De Palma, R.; Peeters, S.; Van Bael, M. J.; Van den Rul, H.; Bonroy, K.; Laureyn, W.; Mullens, J.; Borghs, G.; Maes, G. Silane Ligand Exchange to Make Hydrophobic Superparamagnetic Nanoparticles Water-Dispersible. *Chem. Mater.* **2007**, *19*, 1821–1831.
10. Yavuz, C. T.; Mayo, J. T.; Yu, W. W.; Prakash, A.; Falkner, J. C.; Yean, S.; Cong, L. L.; Shipley, H. J.; Kan, A.; Tomson, M.; *et al.* Low-Field Magnetic Separation of Monodisperse Fe_3O_4 Nanocrystals. *Science* **2006**, *314*, 964–967.
11. Kim, S. J.; Wi, H. S.; Kim, K.; Lee, K.; Kim, S. M.; Yang, H. S.; Pak, H. K. Encapsulation of CdSe Nanoparticles inside Liposome Suspended in Aqueous Solution. *J. Korean Phys. Soc.* **2006**, *49*, S684−S687.

12. Bruchez, M.; Moronne, M.; Gin, P.; Weiss, S.; Alivisatos, A. P. Semiconductor Nanocrystals as Fluorescent Biological Labels. *Science* **1998**, *281*, 2013–2016.
13. Chan, W. C. W.; Nie, S. M. Quantum Dot Bioconjugates for Ultrasensitive Nonisotopic Detection. *Science* **1998**, *281*, 2016–2018.
14. Michalet, X.; Pinaud, F. F.; Bentolila, L. A.; Tsay, J. M.; Doose, S.; Li, J. J.; Sundaresan, G.; Wu, A. M.; Gambhir, S. S.; Weiss, S. Quantum Dots for Live Cells, *in Vivo* Imaging, and Diagnostics. *Science* **2005**, *307*, 538–544.
15. Rembaum, A. U.S. Patent Specification 4267234. 1983.
16. Yu, W. W.; Chang, E.; Sayes, C. M.; Drezek, R.; Colvin, V. L. Aqueous Dispersion of Monodisperse Magnetic Iron Oxide Nanocrystals through Phase Transfer. *Nanotechnology* **2006**, *17*, 4483–4487.
17. Chen, Y.; Thakar, R.; Snee, P. T. Imparting Nanoparticle Function with Size-Controlled Amphiphilic Polymers. *J. Am. Chem. Soc.* **2008**, *130*, 3744–3745.
18. Veiga, V.; Ryan, D. H.; Sourty, E.; Llanes, F.; Marchessault, R. H. Formation and Characterization of Superparamagnetic Cross-Linked High Amylose Starch. *Carbohydr. Polym.* **2000**, *42*, 353–357.
19. Sun, S. H.; Zeng, H.; Robinson, D. B.; Raoux, S.; Rice, P. M.; Wang, S. X.; Li, G. X. Monodisperse MFe_2O_4 (M = Fe, Co, Mn) Nanoparticles. *J. Am. Chem. Soc.* **2004**, *126*, 273–279.
20. Lattuada, M.; Hatton, T. A. Functionalization of Monodisperse Magnetic Nanoparticles. *Langmuir* **2007**, *23*, 2158–2168.
21. Wooding, A.; Kilner, M.; Lambrick, D. B. Studies of the Double Surfactant Layer Stabilization of Water-Based Magnetic Fluids. *J. Colloid Interface Sci.* **1991**, *144*, 236–242.
22. Evident_Technologies. Cdse/Zns Evitags, Type 1 and Type 2-MP MSDS V1.1 *http://www.evidenttech.com/assets/docs/MSDS/CdSe-ZnS-T1-T2-EviTags-MSDS-v2.pdf* [Online], January 2006.
23. Aldana, J.; Wang, Y. A.; Peng, X. G. Photochemical Instability of CdSe Nanocrystals Coated by Hydrophilic Thiols. *J. Am. Chem. Soc.* **2001**, *123*, 8844–8850.
24. Yu, W. W.; Chang, E.; Falkner, J. C.; Zhang, J. Y.; Al-Somali, A. M.; Sayes, C. M.; Johns, J.; Drezek, R.; Colvin, V. L. Forming Biocompatible and Nonaggregated Nanocrystals in Water Using Amphiphilic Polymers. *J. Am. Chem. Soc.* **2007**, *129*, 2871–2879.
25. Choi, H. S.; Ipe, B. I.; Misra, P.; Lee, J. H.; Bawendi, M. G.; Frangioni, J. V. Tissue- and Organ-Selective Biodistribution of NIR Fluorescent Quantum Dots. *Nano. Lett* **2009**, *9*, 2354–2359.
26. Xie, R.; Chen, K.; Chen., X.; Peng, X. InAs/InP/ZnSe Core/Shell/Shell Quantum Dots as near-Infrared Emitters: Bright, Narrow-Band, Non-Cadmium Containing, and Biocompatible. *Nano. Res.* **2008**, *1*, 457–464.
27. Pisanic, T. R.; Blackwell, J. D.; Shubayev, V. I.; Finones, R. R.; Jin, S. Nanotoxicity of Iron Oxide Nanoparticle Internalization in Growing Neurons. *Biomaterials* **2007**, *28*, 2572–2581.
28. Hilger, I.; Fruhauf, S.; Linss, W.; Hiergeist, R.; Andra, W.; Hergt, R.; Kaiser, W. A. Cytotoxicity of Selected Magnetic Fluids on Human Adenocarcinoma Cells. *J. Magn. Magn. Mater.* **2003**, *261*, 7–12.
29. Lacava, Z. G. M.; Azevedo, R. B.; Martins, E. V.; Lacava, L. M.; Freitas, M. L. L.; Garcia, V. A. P.; Rebula, C. A.; Lemos, A. P. C.; Sousa, M. H.; Tourinho, F. A.; *et al.* Biological Effects of Magnetic Fluids: Toxicity Studies. *J. Magn. Magn. Mater.* **1999**, *201*, 431–434.
30. Shen, A. Q.; Gleason, B.; McKinley, G. H.; Stone, H. A. Fiber Coating with Surfactant Solutions. *Phys. Fluids* **2002**, *14*, 4055–4068.
31. Linse, S.; Cabaleiro-Lago, C.; Xue, W. F.; Lynch, I.; Lindman, S.; Thulin, E.; Radford, S. E.; Dawson, K. A. Nucleation of Protein Fibrillation by Nanoparticles. *Proc. Natl. Acad. Sci. U.S.A.* **2007**, *104*, 8691–8696.
32. Shimoiizaka, J.; Nakatsuka, K.; Fujita, T.; Kounosu, A. Sink-Float Separators Using Permanent-Magnets and Water-Based Magnetic Fluid. *IEEE Trans. Magn.* **1980**, *16*, 368–371.
33. Khalafalla, S. E.; Reimers, G. W. Preparation of Dilution-Stable Aqueous Magnetic Fluids. *IEEE Trans. Magn.* **1980**, *16*, 178–183.
34. Decuyper, M.; Joniau, M. Magnetoliposomes—Formation and Structural Characterization. *Eur. Biophys. J. Biophys. Lett.* **1988**, *15*, 311–319.
35. Morales, M. A.; Jain, T. K.; Labhasetwar, V.; Leslie-Pelecky, D. L. Magnetic Studies of Iron Oxide Nanoparticles Coated with Oleic Acid and Pluronic (R) Block Copolymer. *J. Appl. Phys.* **2005**, *97*.
36. Young, A. J. Oleic Acid, Chemical Laboratory Information Profile. *J. Chem. Educ.* **2002**, *79*.
37. Landfester, K.; Ramirez, L. P. Encapsulated Magnetite Particles for Biomedical Application. *J. Phys.: Condens. Matter* **2003**, *15*, S1345−S1361.
38. Murakami, K.; Chan, S. Y.; Routtenberg, A. Protein-Kinase-C Activation by Cis-Fatty Acid in the Absence of Ca^{2+} and Phospholipids. *J. Biol. Chem.* **1986**, *261*, 5424–5429.
39. Jakubowski, H. *Biochemistry Online: An Approach Based on Chemical Logic*. http://employees.csbsju.edu/hjakubowski/classes/ch331/bcintro/default.html (accessed December 2008).
40. Dabbousi, B. O.; RodriguezViejo, J.; Mikulec, F. V.; Heine, J. R.; Mattoussi, H.; Ober, R.; Jensen, K. F.; Bawendi, M. G. (Cdse)Zns Core−Shell Quantum Dots: Synthesis and Characterization of a Size Series of Highly Luminescent Nanocrystallites. *J. Phys. Chem. B* **1997**, *101*, 9463–9475.
41. *Particle/Pore Size Analysis Software Instruction Manual*. *Nanosolver,* version 3.4; Rigaku-Corporation: Wooldands, TX, 2006.
42. Watanabe, J.; Ono, H.; Uematsu, I.; Abe, A. Thermotropic Polypeptides. 2. Molecular Packing and Thermotropic Behavior of Poly(L-Glutamates) with Long Normal-Alkyl Side-Chains. *Macromolecules* **1985**, *18*, 2141–2148.
43. Zhang, L. W.; Yu, W. W.; Colvin, V. L.; Monteiro-Riviere, N. A. Biological Interactions of Quantum Dot Nanoparticles in Skin and in Human Epidermal Keratinocytes. *Toxicol. Appl. Pharmacol.* **2008**, *228*, 200–211.
44. Gao, X. H.; Cui, Y. Y.; Levenson, R. M.; Chung, L. W. K.; Nie, S. M. *In Vivo* Cancer Targeting and Imaging with Semiconductor Quantum Dots. *Nat. Biotechnol.* **2004**, *22*, 969–976.
45. Levasseur, B.; Renard, B.; Barbier, J.; Duprez, D. Catalytic Wet Air Oxidation of Oleic Acid on Ceria-Supported Platinum Catalyst. Effect of pH. *React. Kinet. Catal. Lett.* **2006**, *87*, 269–279.
46. Travert-Branger, N.; Dubois, F.; Carion, O.; Carrot, G.; Mahler, B.; Dubertret, B.; Doris, E.; Mioskowski, C. Oligomeric PEG-Phospholipids for Solubilization and Stabilization of Fluorescent Nanocrystals in Water. *Langmuir* **2008**, *24*, 3016–3019.
47. Hyeon, T.; Lee, S. S.; Park, J.; Chung, Y.; Bin Na, H. Synthesis of Highly Crystalline and Monodisperse Maghemite Nanocrystallites without a Size-Selection Process. *J. Am. Chem. Soc.* **2001**, *123*, 12798–12801.
48. Yu, W. W.; Peng, X. G. Formation of High-Quality CdS and Other II−VI Semiconductor Nanocrystals in Noncoordinating Solvents: Tunable Reactivity of Monomers. *Angew. Chem., Int. Ed.* **2002**, *41*, 2368–2371.
49. Yu, W. W.; Qu, L. H.; Guo, W. Z.; Peng, X. G. Experimental Determination of the Extinction Coefficient of CdTe, CdSe, and CdS Nanocrystals. *Chem. Mater.* **2003**, *15*, 2854–2860.